Robotica (2018) volume 36, pp. 1098–1109. © Cambridge University Press 2018
doi:10.1017/S0263574718000279

Singularities of a planar 3-RPR parallel manipulator with joint clearance

Marise Gallant†* and Clément Gosselin‡

†*Université de Moncton, Moncton, NB, Canada*
‡*Université Laval, Québec, Canada. E-mail: gosselin@gmc.ulaval.ca*

(Accepted March 10, 2018. First published online: April 2, 2018)

SUMMARY
If the joint clearances of the joints of a manipulator are considered, an unconstrained motion of the end-effector can be computed. This is true for all poses of the manipulator, even with all actuators locked.

This paper presents how this unconstrained motion can be determined for a planar 3-RPR manipulator. The singularities are then studied. It is shown that when clearances are considered, the singularity curves normally found in the workspace of such a manipulator become singular zones. These zones can be significant and greatly reduce the usable workspace of a manipulator. Since a prescribed configuration that would not, in theory, corresponds to a singular pose can become singular due to the unconstrained motion, the results of this paper are relevant to manipulator design and trajectory planning.

KEYWORDS: Joint clearance; Singularities; Parallel manipulator.

1. Introduction

Many researchers have worked on the optimization of kinematic properties and the identification of singular configurations. These configurations result in an instantaneous change of degrees of freedom (DOF), loss of control, and a degradation of much sought kinematic properties of parallel manipulators. Different works can be found on the study of singular configurations, on their classification, on their computation, and on their avoidance.

Gosselin and Angeles[1] classify singularities of parallel manipulators into three types, based on the Jacobian matrices. The first type corresponds to the workspace boundary and to boundaries inside the workspace that separate regions that do not have the same number of solutions to the inverse kinematic problem (IKP). The inverse Jacobian matrix is then singular. The second type, where the direct Jacobian matrix is singular, may occur inside the workspace, and the third type, often called *architectural* (certain special geometrical parameters are needed), can be avoided at the design stage. In this case, both Jacobian matrices are singular simultaneously. Zlatanov, Fenton and Benhabib[2,3] have compiled and grouped singularities into 6 types and 21 classes using velocity equations. This classification is exhaustive. For the planar 3-RPR (revolute-actuated prismatic-revolute) studied here, all possible singular configurations can be obtained using the simpler classification of Gosselin and Angeles,[1] where only the Jacobian matrices are needed. Also, since this architecture is well-known, the singularity equations have already been obtained.[4,5] Singularity curves have also been superimposed onto the cartesian workspace, for best interpretation of the results.[4,6,7]

In order to avoid singularities, some work exists on trajectory planning,[8–10] on redundant actuation,[11–13] and even on adding braking systems at the passive joints.[14] Other works focus on parallel manipulator synthesis in order to obtain architectures having singularity-free workspaces.[15,16]

A source of error of the position and orientation accuracy is the clearance in the joints. Researchers agree on the necessity to study joint clearances.[17–22] Calibration of manipulators can compensate for

* Corresponding author. E-mail: marise.gallant@umoncton.ca

errors caused by the link dimensional tolerance, since these errors are predictable. For this reason, some say joint clearance is a more important source of error.[20]

In two-dimensional (2D), joint clearances in revolute joints are modeled in different manners. Ting, Zhu and Watkins[23] model clearances by replacing each of the joints with an additional actuated link having a length equal to half of the clearance. Their model is used to geometrically determine the largest possible errors. Tsai and Lai[24,25] and Ting, Hsu, Yu and Wang[22] also model clearance in revolute joints by replacing them with links, but these are not actuated.

Other authors include the effect of clearances by varying the length of certain links and obtain a workspace when the actuators are locked.[19,26,27] This approach is used in this paper, where the leg lengths vary according to the clearance of the passive revolute joints. The workspaces are obtained with the algorithm presented in ref. [28],where the boundaries of a constant orientation workspace are composed of arcs for the manipulator studied. The method is easy to implement in a computer algorithm.

The errors due to joint clearance vary inside the workspace. These errors are included inside an *unconstrained workspace*, which can be obtained at any prescribed posture of the manipulator. The unconstrained workspace represents the possible movement of the end-effector when the actuators are locked. For task or trajectory planning, it is important to know how these errors can affect kinematic properties, especially the location of singular configurations.

The workspace of a manipulator without joint clearances may contain singularity curves. When considering finite values of clearance, these same singularity curves become singularity zones. Knowing where these zones are located may greatly help task or trajectory planning, and even the design of a manipulator.

In this paper, the planar 3-RPR parallel manipulator is considered and its kinematics are briefly recalled. Then, the constant orientation workspace is calculated, as well as the Jacobian matrices. Algorithms are presented to obtain the unconstrained workspace of the manipulator, which will be useful to compute singularity zones of the manipulator. In Section 3, a joint clearance model is presented, as well as the computation of the resulting unconstrained workspace. In Section 4, the algorithm used to obtain the singularity zones is explained. Results are then presented, followed by the conclusions.

2. The Planar Three-Degree-of-Freedom Parallel Manipulator

The manipulator studied in this paper is well-known. This section recalls the geometry, workspace, and velocity equations needed to study the effects of joint clearances on the singular configurations of the manipulator.

2.1. Geometry and inverse kinematic problem (IKP)

The manipulator is shown in Fig. 1. The geometry of the base is defined by the position vectors $\mathbf{r}_1$, $\mathbf{r}_2$, and $\mathbf{r}_3$ of the fixed revolute joints expressed in a fixed reference frame: Oxy. The geometry of the mobile platform is defined by three vectors: $\mathbf{s}_{10}$, $\mathbf{s}_{20}$, and $\mathbf{s}_{30}$, giving the position of the mobile revolute joints and expressed in the reference frame $O'x'y'$, which is attached to the mobile platform at the end-effector. These same vectors are denoted $\mathbf{s}_i$, $i = 1, 2, 3$ when expressed in the fixed reference frame.

The mobile platform is connected to the fixed base via three identical RPR kinematic chains, where the prismatic joint is actuated. Vectors $\mathbf{u}_i$, $i = 1, 2, 3$ are along the length of the prismatic joints and originate at the fixed revolute joints on the base. The length of each actuator (which is assumed to be positive) is given by ρ_1, ρ_2, and ρ_3, which are the lengths of vectors $\mathbf{u}_i$, $i = 1, 2, 3$. The output can be expressed as the position vector $\mathbf{p} = [x, y]^{\mathrm{T}}$ and the rotation matrix $\mathbf{Q}$:

$$\mathbf{Q} = \begin{bmatrix} \cos\phi & -\sin\phi \\ \sin\phi & \cos\phi \end{bmatrix}, \tag{1}$$

where ϕ is the orientation of $O'x'y'$ with respect to Oxy.

https://doi.org/10.1017/S0263574718000279 Published online by Cambridge University Press

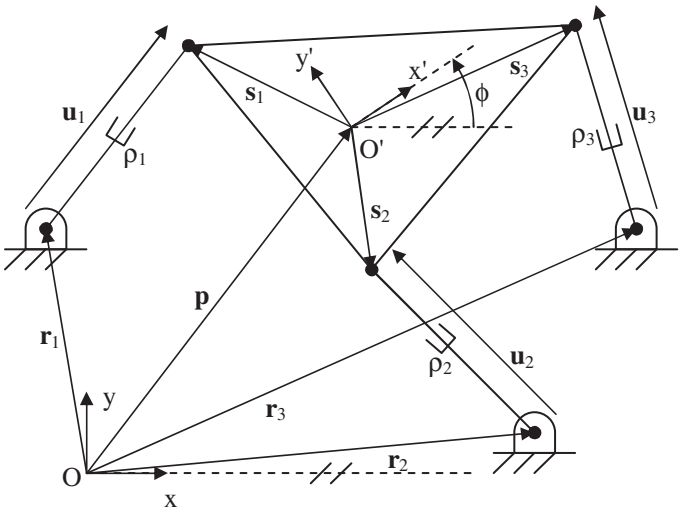

Fig. 1. The 3-RPR planar parallel manipulator.

For each of the kinematic chains, the solution to the IKP is given by

$$\rho_i^2 = \mathbf{u}_i^{\mathrm{T}}\mathbf{u}_i = (\mathbf{p} + \mathbf{s}_i - \mathbf{r}_i)^{\mathrm{T}}(\mathbf{p} + \mathbf{s}_i - \mathbf{r}_i), \quad i = 1, 2, 3, \tag{2}$$

2.2. Workspace

The most common type of workspace for planar 3-DOF manipulators is the constant orientation workspace. For a constant orientation, where vectors $\mathbf{s}_i$, $i = 1, 2, 3$ are fixed, the constant orientation workspace is the intersection of three annular regions, each composed of two concentric circles, centered at the end of vectors $\mathbf{r}_i - \mathbf{s}_i$, $i = 1, 2, 3$. The inner and outer radii correspond to the minimum and maximum actuated leg lengths $\rho_{i,\min}$ and $\rho_{i,\max}$, respectively, for $i = 1, 2, 3$. To obtain an x, y, ϕ workspace, the orientation ϕ can be varied and the constant orientation workspace obtained at each value of ϕ. This is useful for determining the unconstrained motion of the manipulator.

2.3. Singularities

The Jacobian matrices are obtained by differentiating the IKP Eq. (2) with respect to time:

$$2\rho_i\dot{\rho}_i = 2(\mathbf{p} + \mathbf{s}_i - \mathbf{r}_i)^{\mathrm{T}}(\dot{\mathbf{p}} + \dot{\mathbf{Q}}\mathbf{s}_{i0}), \quad i = 1, 2, 3. \tag{3}$$

With

$$\mathbf{p} + \mathbf{s}_i - \mathbf{r}_i = \mathbf{u}_i \quad \text{and} \quad \dot{\mathbf{Q}}\mathbf{s}_{i0} = \dot{\phi}\mathbf{E}\mathbf{Q}\mathbf{s}_{i0}, \tag{4}$$

where

$$\mathbf{E} = \begin{bmatrix} 0 & -1 \\ 1 & 0 \end{bmatrix}, \tag{5}$$

Eq. (3) can be written in matrix form:

$$\mathbf{A}[\dot{\rho}_1 \quad \dot{\rho}_2 \quad \dot{\rho}_3]^{\mathrm{T}} = \mathbf{B}[\dot{\mathbf{p}} \quad \dot{\phi}]^{\mathrm{T}}, \tag{6}$$

where

$$\mathbf{A} = \begin{bmatrix} \rho_1 & 0 & 0 \\ 0 & \rho_2 & 0 \\ 0 & 0 & \rho_3 \end{bmatrix} \quad \text{and} \quad \mathbf{B} = \begin{bmatrix} \mathbf{u}_1^{\mathrm{T}} & \mathbf{u}_1^{\mathrm{T}}\mathbf{E}\mathbf{Q}\mathbf{s}_{10} \\ \mathbf{u}_2^{\mathrm{T}} & \mathbf{u}_2^{\mathrm{T}}\mathbf{E}\mathbf{Q}\mathbf{s}_{20} \\ \mathbf{u}_3^{\mathrm{T}} & \mathbf{u}_3^{\mathrm{T}}\mathbf{E}\mathbf{Q}\mathbf{s}_{30} \end{bmatrix}. \tag{7}$$

https://doi.org/10.1017/S0263574718000279 Published online by Cambridge University Press

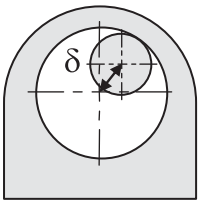

Fig. 2. Clearance in a passive revolute joint.

Matrix **B** is singular when vectors $\mathbf{u}_1, \mathbf{u}_2$, and $\mathbf{u}_3$ intersect at one point or at infinity (parallel). These singularities are of type II[1] and can be located inside the workspace. The locus of the singularities in the workspace is obtained by writing det $(\mathbf{B}) = 0$. For this manipulator, the equations are quadratic for a constant orientation:[4]

$$E_1x^2 + E_2y^2 + E_3xy + E_4x + E_5y = 0, \tag{8}$$

where coefficients E_i, $i = 1, 2, \ldots, 5$ are a function of the orientation and the geometry of the manipulator (vectors $\mathbf{r}_i$ and $\mathbf{s}_{i0}$, $i = 1, 2, 3$).

3. Unconstrained Workspace Caused by Joint Clearance

This section first presents how the clearance is modeled inside the passive revolute joints and its effect on each leg. It is then shown what unconstrained motion of the end-effector is possible when the actuators are locked. The unconstrained motion of the end-effector, caused by clearance, may cause an important degradation of the global properties of the manipulators. The aim of this study is to find all configurations that may become singular due to joint clearance.

3.1. Joint clearance model

Figure 2 shows the simple 1-DOF clearance model chosen for the passive revolute joints. The clearance is defined as the distance between the center of the pin and the center of the hole, when there is contact in the joint.

When the prismatic actuators are locked, each RPR leg becomes an RR kinematic chain. Then, the clearance of each revolute joint is considered (δ_1 and δ_2). The total possible variation of each leg length due to clearances is 2δ, where $\delta = \delta_1 + \delta_2$. This result can be applied in the same manner to a SPS (S for spherical) kinematic chain, which becomes a SS kinematic chain when the prismatic actuator is locked.

For the remainder of this paper, δ designates the combination of the passive joint clearances. For the determination of the unconstrained workspace (when the actuators are locked), the following minimum and maximum leg lengths will be used for $i = 1, 2, 3$:

$$\begin{array}{ll} \rho_i - \delta & \text{minimum leg length} \\ \rho_i + \delta & \text{maximum leg length.} \end{array} \tag{9}$$

Some authors vary the link lengths of manipulators in the same manner as presented here in order to model the clearance present in the joints.[19,26,27] Others obtain the position error at the end-effector due to errors in the actuators.[29,30] This is similar to the approach used here when the actuators are prismatic, but the authors specify that their method is valid when used in a singularity-free area of the workspace. In this paper, the clearance is modeled at singular configurations.

3.2. Unconstrained workspace

The unconstrained workspace represents the possible movement of the end-effector when the actuators are locked. It can be obtained for any prescribed pose of the end-effector. The unconstrained workspace is obtained in the same manner as the workspace of the manipulators, by substituting the minimum and maximum prismatic actuator lengths with the corresponding values defined in Eq. (9). If this workspace is composed of more than one piece (not simply connected), only the one containing the

https://doi.org/10.1017/S0263574718000279 Published online by Cambridge University Press

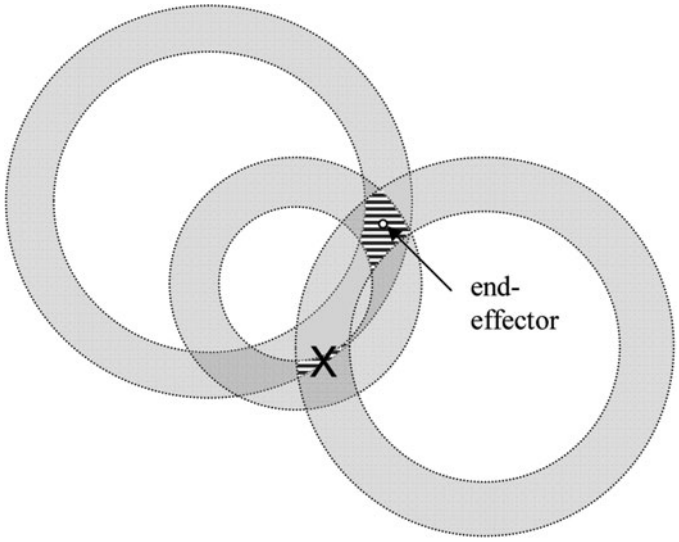

Fig. 3. Unconnected unconstrained workspace.

initial chosen position is truly the unconstrained workspace, as the end-effector cannot move from one to the other. An example is shown in Fig. 3, where the workspace obtained is composed of two separate areas, highlighted with black and white stripes. The area where the end-effector is identified is the true unconstrained workspace. Therefore, the other area marked with an X is the area to eliminate.

The boundaries of the workspace is defined by a list of arcs. The following steps are used to select and keep only the arcs that make up the true unconstrained workspace:

1. Determine which arc is closest to the end-effector. This arc becomes the first arc of the list of arcs that will define the boundaries of the unconstrained workspace. One of its ends becomes the starting point.
2. Search remaining arcs to find one adjacent to the last arc added to the list. Add to the list.
3. Determine if last arc added closes the loop by joining the very first arc of the list. In the affirmative: stop, otherwise go to previous step.

At this point, only constant-orientation workspaces have been considered. Since the orientation of the end-effector is also unconstrained, an $xy\phi$ unconstrained workspace must be obtained. This is possible by discretizing the value of the orientation ϕ. The increment ($\triangle\phi$) must be sufficiently small to resemble the actual $xy\phi$ unconstrained workspace, but large enough to minimize computation time. The value of $\triangle\phi$ must be carefully chosen for each architecture.

For each value of ϕ, arcs that are not part of the unconstrained workspace must be eliminated as described above. Furthermore, the unconstrained workspaces of two consecutive values of ϕ must be connected for the end-effector to rotate from one orientation to the other. To verify this, the existence of the intersection of these workspaces, projected on the same xy-plane of the $xy\phi$ configuration space, is verified. If this intersection exists, the two workspaces are considered to be connected.

Figure 4 illustrates an example of *connected consecutive workspaces*, when projected on the same plane. The following algorithm is used to check for an intersection of two workspaces:

1. Have a list of arcs, *arcs1*, defining the boundaries of an unconstrained workspace.
2. Obtain a list of arcs, *arcs2*, defining the boundaries of a second unconstrained workspace.
3. Verify if at least one arc of list *arcs2* intersects one of the arcs from list *arcs1*. If yes: stop, an intersection of the workspaces exists.
4. Verify if any arc of list *arcs2* is inside the boundaries defined by *arcs1*. If yes: stop, an intersection of the workspaces exists.
5. Verify if any arc of list *arcs1* is inside the boundaries defined by *arcs2*. If yes: stop, an intersection of the workspaces exists.
6. There is no intersection of the workspaces.

https://doi.org/10.1017/S0263574718000279 Published online by Cambridge University Press

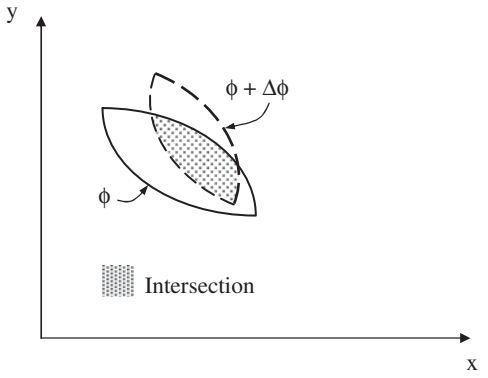

Fig. 4. Workspaces obtained for two consecutive values of ϕ projected onto the xy-plane.

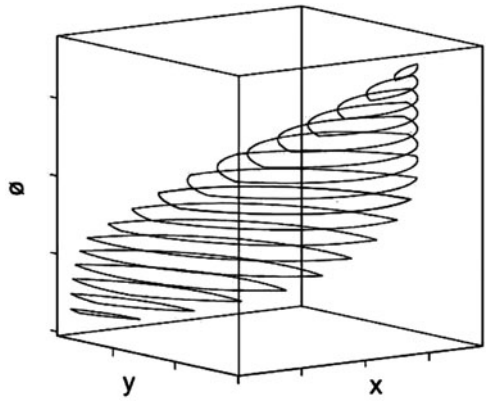

Fig. 5. $xy\phi$ unconstrained workspace of the manipulator for a chosen position and orientation of the end-effector.

The $xy\phi$ unconstrained workspace of Fig. 5 shows no discontinuities and is entirely connected. The end-effector could thus reach any point of any orientation shown.

The shape and size of $xy\phi$ unconstrained workspaces vary for different $xy\phi$ values inside the workspace of the 3-RPR manipulator. This unconstrained motion will cause position and orientation errors of the end-effector. Kinematic properties of the manipulator will vary. The worst case scenario is when the unconstrained motion of the manipulator in a non-singular configuration may allow the manipulator to reach a singular configuration under the action of certain external forces or moments. This possibility exists if the three-dimensional (3D) unconstrained workspace intersects the singularity manifold.

For trajectory planning, it is thus important not only to avoid singularity curves located inside the workspace, but also all configurations that may become singular, which will be called singularity zones henceforth. The following section explains how all singular zones are identified.

4. Algorithm for Obtaining Singularities

The algorithm presented here is useful for identifying the areas of the workspace where the manipulator may reach a singular configuration, and allow for a clearance-free planning of tasks in the singularity-free part of the workspace. It is therefore useful in choosing a singularity-free trajectory inside of the workspace.

The methods proposed here are based on the following principle: *At a given point A of the workspace of the 3-RPR, the unconstrained workspace is obtained and includes a point B. If, at this point B, the unconstrained workspace is obtained, it will include point A.* This is illustrated in Fig. 6 for a planar 2-DOF manipulator, where points A and B are inside both unconstrained workspaces. The same is true

https://doi.org/10.1017/S0263574718000279 Published online by Cambridge University Press

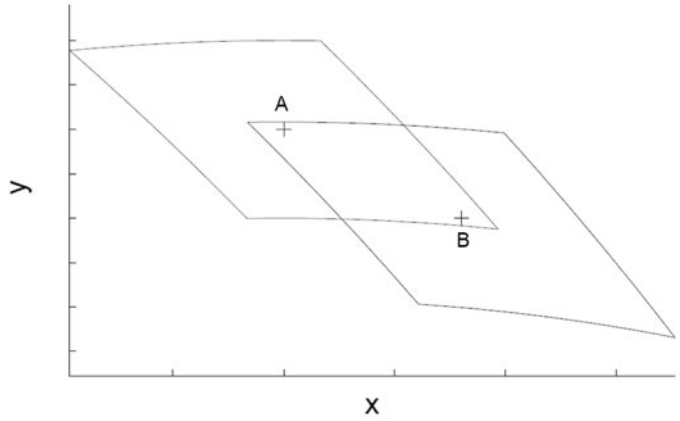

Fig. 6. Two points, A and B, each with their respective unconstrained workspaces.

for the 3-RPR manipulator. If point B is chosen inside the $xy\phi$ unconstrained workspace computed at point A, point A would be included in the $xy\phi$ unconstrained workspace computed at point B.

The inverse kinematic solution of point A will be included in the $[\rho_i - \delta,\ \rho_i + \delta]$, $i = 1, 2, 3$ intervals obtained from the inverse kinematic solution of point B and vice-versa. Most importantly, if point A represents a singularity and an unconstrained workspace is obtained, any point B included in this workspace will represent a potential singular configuration as its own unconstrained workspace will include the singular point A. Point B is thus part of the singularity zone. The search for all the areas constituting the singularity zone will therefore originate on the singularity manifold.

The goal is to obtain the singularity zones of a constant orientation workspace ($\phi = \phi_{\text{chosen}}$). However, since the unconstrained workspace is a region of the 3D $xy\phi$ space, the unconstrained rotation is considered when determining whether a $xy\phi_{\text{chosen}}$ point is inside the singularity zone. For incrementing values of ϕ, the singularity curves are obtained and discretized to obtain a list of xy points at which the unconstrained motion is computed. If, at any value of ϕ, the 3D $xy\phi$ unconstrained workspace of a singular xy point contains the originally chosen orientation (ϕ_{chosen}), the corresponding 2D xy slice of the 3D $xy\phi$ unconstrained workspace is part of the singularity zone.

The following four steps of the algorithm, repeated in a loop with incrementing values of ϕ, add to the singularity zone until it is complete. The value of ϕ starts at ϕ_{chosen} and increases by $\Delta\phi$ with each cycle through the loop until an orientation that contributes nothing to the singularity zone is reached. The value of ϕ is then reset to ϕ_{chosen} and decreased by $\Delta\phi$ with each cycle through the loop until an orientation that contributes nothing to the singularity zone is reached. The singularity zone will then be complete. These are the steps to execute at each value of ϕ:

1. Obtain the singularity curve and discretize to obtain list of points (x_i, y_i), $i = 1 \ldots n$.
2. For each of the n points, obtain leg lengths ρ_1, ρ_2, and ρ_3.
3. For each of the n points, obtain 3D $xy\phi$ unconstrained workspace.
4. For each of the n points, verify if $xy\phi$ unconstrained workspace contains a xy slice corresponding to ϕ_{chosen}. In the affirmative, add xy slice to singularity zone.

At the first cycle through the loop, steps 1 and 2 remain the same. However, steps 3 and 4 are simplified as the value of ϕ is ϕ_{chosen}: the n 2D $xy\phi_{\text{chosen}}$ unconstrained workspaces are computed and plotted on the constant orientation workspace, as their union will constitute part of the final singularity zone. Figure 7 shows this preliminary result. At this stage, the unconstrained rotation of the end-effector has not yet been considered. In the example of Fig. 7, the singularity curve is an ellipse. The unconstrained workspaces are shown for different points of the ellipse. The corresponding constant orientation workspace of the manipulator is also shown.

5. Results

The singularity zones include all positions (for a chosen orientation) of the end-effector that may allow the manipulator to reach a singular configuration. Outside of these zones, it is impossible

https://doi.org/10.1017/S0263574718000279 Published online by Cambridge University Press

Table I. Architecture of the planar 3-RPR manipulator.

Fixed base	Mobile platform
$\mathbf{r}_1 = [0 \quad 0]^T$	$\mathbf{s}_{01} = [-0.2 \quad -0.2]^T$
$\mathbf{r}_2 = [1 \quad 0]^T$	$\mathbf{s}_{02} = [0.2 \quad 0]^T$
$\mathbf{r}_3 = [0 \quad 1]^T$	$\mathbf{s}_{03} = [-0.1 \quad 0.3]^T$

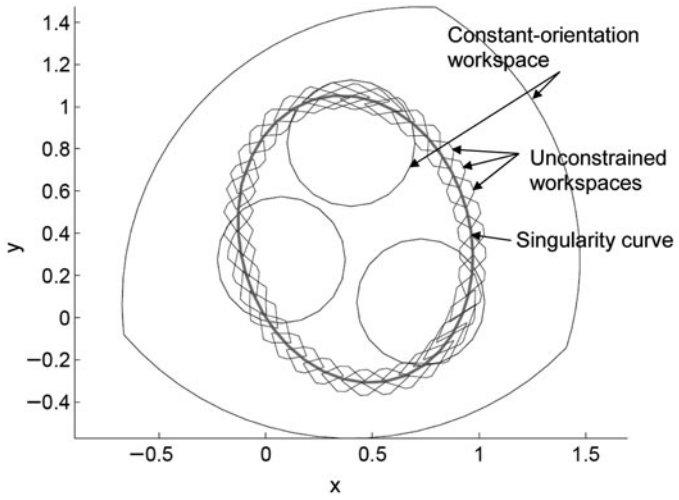

Fig. 7. The singularity zone obtained before the unconstrained rotation of the end-effector is considered.

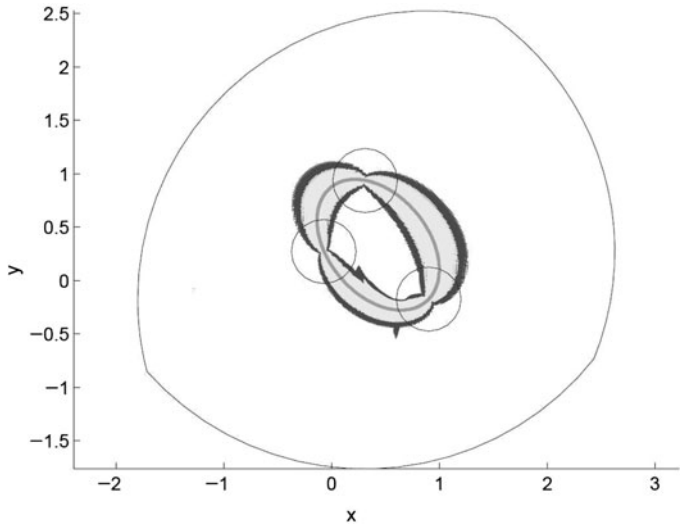

Fig. 8. Singularity curve obtained with a constant orientation $\phi = 60^\circ$ and the singularity zones corresponding to $\delta = 0.1$ and $\delta = 0.2$.

for the manipulator to reach a singular configuration. All the following results were obtained using Matlab®.

The fixed base of the planar 3-RPR is defined by vectors $\mathbf{r}_1$, $\mathbf{r}_2$, and $\mathbf{r}_3$ presented in Table I. The mobile platform is described by vectors $\mathbf{s}_{01}$, $\mathbf{s}_{02}$, and $\mathbf{s}_{03}$, expressed in the mobile reference frame attached to the mobile platform. The minimum and maximum leg lengths are $\rho_{\min} = 0.3$ and $\rho_{\max} = 2.7$, respectively, and are identical for ρ_i, $i = 1, 2, 3$. The results presented are obtained with this architecture.

Figure 8 shows, for an orientation of 60°, the effect of the value of δ on the spread of the singularity zone.

https://doi.org/10.1017/S0263574718000279 Published online by Cambridge University Press

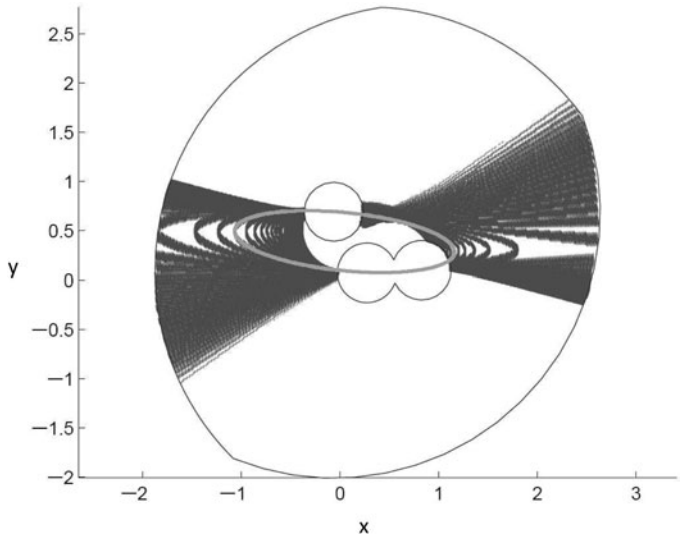

Fig. 9. Singularity curve for $\phi = -30^\circ$ and the singularity zone when $\delta = 0.1$.

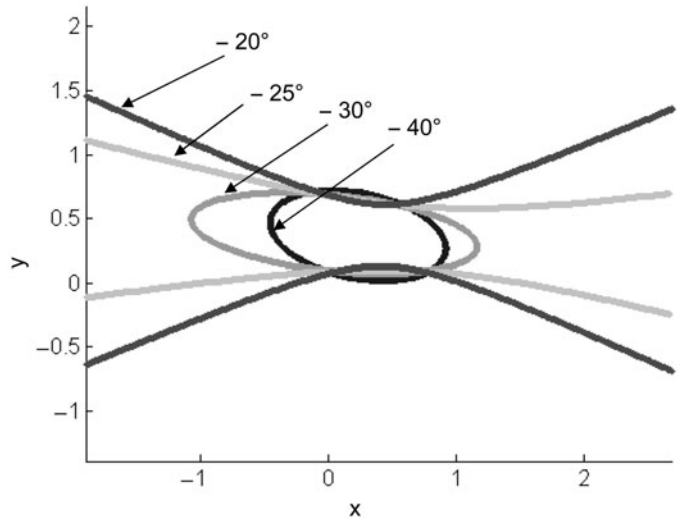

Fig. 10. Singularity curves for $\phi = -40^\circ$, -30°, -25°, and -20°.

The smaller paler zone corresponds to $\delta = 0.1$ and the larger darker zone corresponds to $\delta = 0.2$. The ellipse corresponds to the singularity curve ($\delta = 0$). The constant orientation workspace is also shown. According to these results, doubling the value of δ does not have the effect of doubling the area of the singularity zone.

Similarly to the case with $\phi = 60^\circ$, the singularity locus for an orientation of -30° is also an ellipse (see Fig. 9). As opposed to the first chosen orientation, the singularity zone for $\delta = 0.1$ is much more extensive and divides the workspace into two unconnected parts. This phenomenon can be explained with the help of Fig. 10. Figure 10 shows how the singularity curve evolves for varying orientations around the chosen value of -30°. For diminishing values of ϕ, the singularity curve continues to be elliptical, as shown in Fig. 10 for $\phi = -40^\circ$. Between values $\phi = -30^\circ$ and $\phi = -25^\circ$, the singularity curve changes from elliptical to hyperbolic. Furthermore, while ϕ varies from -30° to -25° (only 5°), the movement of the curve sweeps a large area.

The same phenomenon occurs on the other side of the elliptical-hyperbolic transition, seen in Fig. 11. At an orientation of 20°, the singularity curve is an ellipse, but the transition to a hyperbola is sufficiently close to influence the shape of the singularity zone when $\delta = 0.2$.

https://doi.org/10.1017/S0263574718000279 Published online by Cambridge University Press

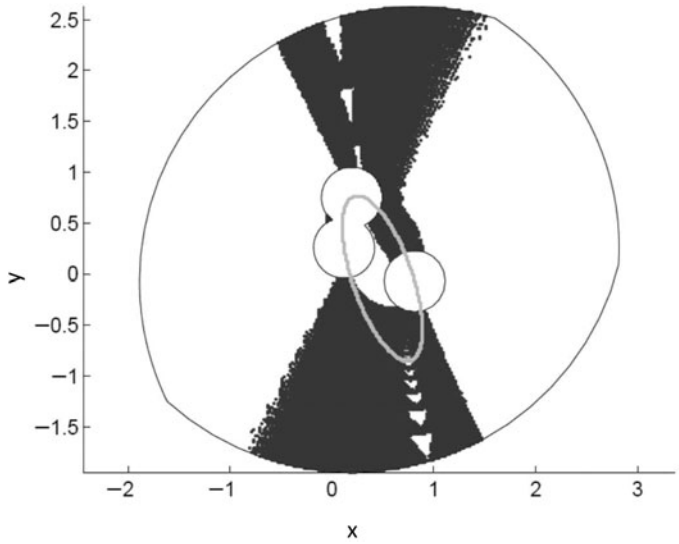

Fig. 11. Singularity curve for $\phi = 20^\circ$ and singularity zone with $\delta = 0.2$.

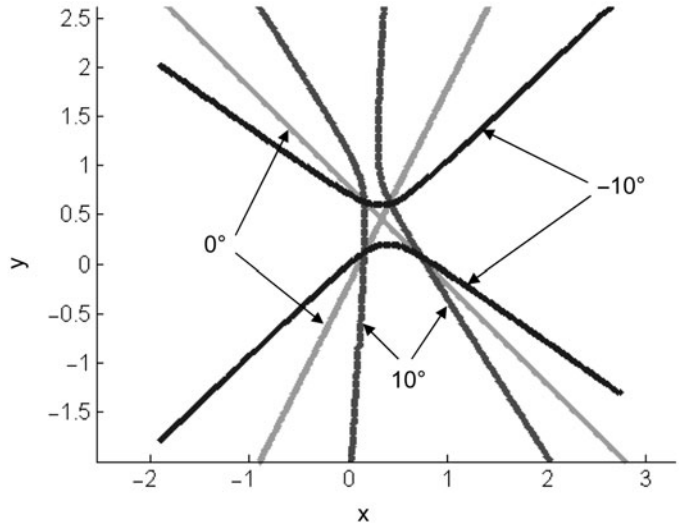

Fig. 12. Singular curves at $\phi = -10^\circ$, 0°, and 10°.

At an orientation of $\phi = 0^\circ$, the singularity curves are two intersecting lines. Figure 12 shows the singularity curves corresponding to orientations $\phi = -10^\circ$, $\phi = 0^\circ$, and $\phi = 10^\circ$. For small variations in orientation, the singularity curves change rapidly. This leads to large singularity zones, when the joint clearances are considered. The usable constant orientation workspace is thus greatly diminished. Figure 13 shows the workspace and the singularity zones when $\delta = 0.2$. The singularity zone is very extensive, compared to the first results shown, when $\phi = 30^\circ$. When planning a given task, it is important to choose an orientation interval as far away as possible from rapid changes in the shape of the singularity curves.

6. Conclusion

The effect of the joint clearances on the singularity configuration was evaluated. Algorithms were presented in order to obtain a connected unconstrained workspace and the singularity zones of a planar 3-RPR manipulator.

https://doi.org/10.1017/S0263574718000279 Published online by Cambridge University Press

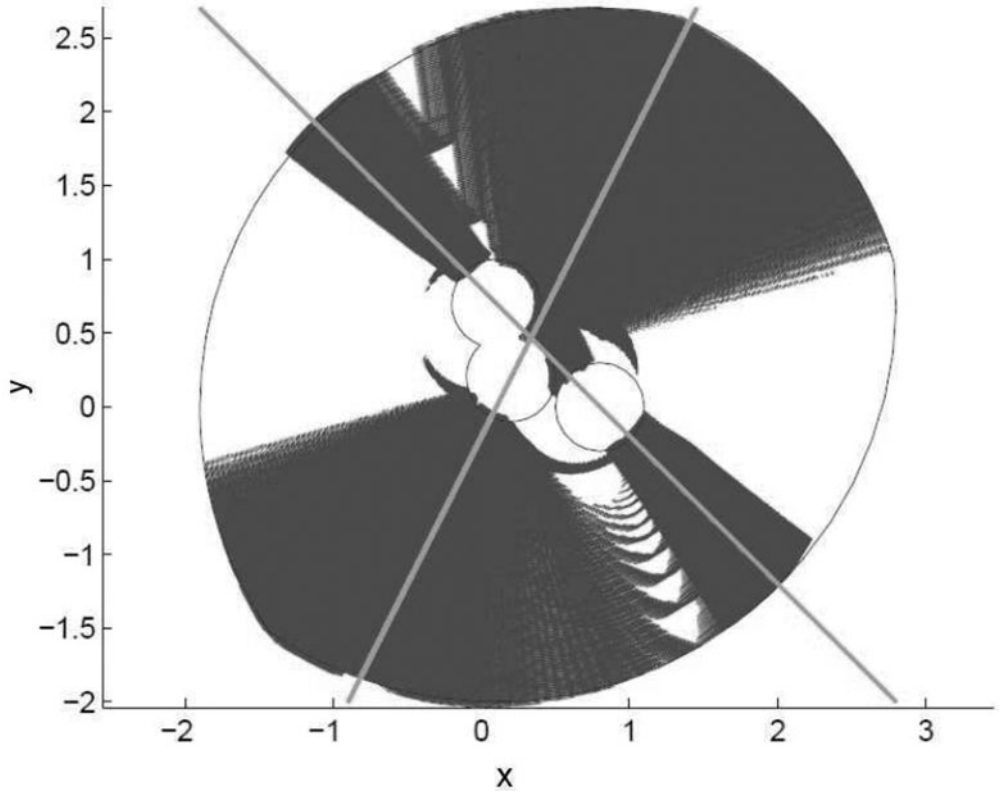

Fig. 13. Singular curves at $\phi = 0^\circ$ and corresponding singularity zone for $\delta = 0.2$.

The singularity zones of the manipulator were presented for chosen orientations and for two different values of δ: $\delta = 0.1$ and $\delta = 0.2$, the effect of the joint clearances. To the author's knowledge, this type of result has not been obtained by others.

Some important observations were made. First, a doubled value of δ did not have the effect of doubling the area of the singularity zone. In fact, the area and shape of the singularity zone did not behave as intuition would predict. Also, the manipulator had relatively small singularity zones for certain orientations and extensive singularity zones at other orientations. It was shown that the size of the singularity zones were related to the rate of change of the shape of the singularity curve in the proximity of the chosen orientation ϕ. The singularity zones were larger if the singularity curves show greater variations in shape for small variations of ϕ. A special case arises at the orientation $\phi = 0^\circ$, where the singularity curves are two intersecting lines. Most of the useful workspace disappears as it is transformed into singularity zones for $\delta = 0.2$.

The algorithm presented here to obtain the singularity zones may be applied to any 3-RPR or 3-SPS manipulator. It may be simplified for a 2-RPR planar manipulator and modified for a n-RPR or n-SPS manipulator.

References

1. C. Gosselin and J. Angeles, "Singularity analysis of closed-loop kinematic chains," *IEEE Trans. Robotic. Autom.* **6**(3), 281–290 (1990).
2. D. Zlatanov, R. G. Fenton and B. Benhabib, "A unifying framework for classification and interpretation of mechanism singularities," *J. Mech. Des.* **117**, 566–572 (1995).
3. D. Zlatanov, R. G. Fenton and B. Benhabib, "Identification and classification of the singular configurations of mechanisms," *Mech. Mach. Theory* **33**(6), 743–760 (1998).
4. J. Sefrioui and C. M. Gosselin, "On the quadratic nature of the singularity curves of planar three-degree-of-freedom parallel manipulators," *Mech. Mach. Theory* **30**(4), 533–551 (1995).
5. I. A. Bonev, D. Zlatanov and C. M. Gosselin, "Singularity analysis of 3-DOF planar parallel mechanisms via screw theory," *J. Mech. Des.* **125**, 573–581 (2003).

https://doi.org/10.1017/S0263574718000279 Published online by Cambridge University Press

6. J. Sefrioui and C. M. Gosselin, "Singularity analysis and representation of planar parallel manipulators," *Robot. Auton. Syst.* **10**, 209–224 (1992).
7. B. Mayer St-Onge and C. M. Gosselin, "Singularity Analysis and Representation of Spatial Six-Degree-of-Freedom Parallel Manipulators," *Proceedings of the 5th International Symposium on Advances in Robot Kinematics (ARK)* (J. Lenarcic and V. Parenti-Castelli, eds.) (Portoroz-Bernardin, Slovénie, 1996) pp. 389–398.
8. S. Bhattacharya, H. Hatwal and A. Ghosh, "Comparison of an exact and an approximate method of singularity avoidance in platform type parallel manipulators," *Mech. Mach. Theory* **33**(7), 965–974 (1998).
9. B. Dasgupta and T. S. Mruthyunjaya, "Singularity-free path planning for the Stewart platform manipulator," *Mech. Mach. Theory* **33**(6), 711–725 (1998).
10. S. Liu, Z.-C. Qiu, and X.-M. Zhang, "Singularity and path-planning with the working mode conversion of a 3-DOF 3-RRR planar parallel manipulator," *Mech. Mach. Theory* **107**, 166–182 (2017).
11. I. Ebrahimi, J. Carretero and R. Boudreau, "A family of kinematically redundant planar parallel manipulators," *ASME J. Mech. Design* **130**(6), 062306.1–062306.8 (2008).
12. R. Matone and B. Roth, "In-Parallel Manipulators: A Framework on How to Model Actuation Schemes and a Study of their Effects on Singular Postures," *Proceedings of ASME DETC'98*, (Atlanta, Georgia) (Sep. 1998) pp. 1–11.
13. M. Carricato and V. Parenti-Castelli, "Kinematics of a family of translational parallel mechanisms with three 4-DOF legs and rotary actuators," *J. Robot. Syst.* **20**(7), 373–389 (2003).
14. J. F. O'Brien and J. T. Wen, "Kinematic Control of Parallel Robots in the Presence of Unstable Singularities," *Proceedings of the 2001 IEEE International Conference on Robotics & Automation*, (Seoul, Korea) (May 21–26 2001).
15. M. Gallant and R. Boudreau, "The synthesis of planar parallel manipulators with prismatic joints for an optimal, singularity-free workspace," *J. Robot. Syst.* **19**(1), 13–24 (2002).
16. M. Arsenault and R. Boudreau, "The synthesis of three-degree-of-freedom planar parallel mechanisms with revolute joints (3-RRR) for an optimal singularity-free workspace," *J. Robot. Syst.* **21**(5), 259–274 (2004).
17. V. Parenti-Castelli and S. Venanzi, "Clearance influence analysis on mechanisms," *Mech. Mach. Theory* **40**, 1316–1329 (2005).
18. C. Innocenti, "Kinematic clearance sensitivity analysis of spatial structures with revolute joints," *Trans. ASME* **124**, 52–57 (2002).
19. P. Voglewede and I. Ebert-Uphoff, "Application of workspace generation techniques to determine the unconstrained motion of parallel manipulators," *J. Mech. Des.* **126**(2), 283–290 (2004).
20. A.-H. Chebbi, Z. Affi and L. Romdhane, "Prediction of the pose errors produced by joints clearance for a 3-UPU parallel robot," *Mech. Mach. Theory* **44**, 1768–1783 (2009).
21. X. Zhang, X. Zhang and Z. Chen, "Dynamic analysis of a 3-RRR parallel mechanism with multiple clearance joints," *Mech. Mach. Theory* **78**, 105–115 (2014).
22. K.-L. Ting, K.-L. Hsu, Z. Yu and J. Wang, "Clearance-induced output position uncertainty of planar linkages with revolute and prismatic joints," *Mech. Mach. Theory* **111**, 66–75 (2017).
23. K.-L. Ting, J. Zhu and D. Watkins, "The effects of joint clearance on position and orientation deviation of linkages and manipulators," *Mech. Mach. Theory* **35**, 391–401 (2000).
24. M.-J. Tsai and T.-H. Lai, "Kinematic sensitivity analysis of linkage with joint clearance based on transmission quality," *Mech. Mach. Theory* **39**, 1189–1206 (2004).
25. M.-J. Tsai and T.-H. Lai, "Accuracy analysis of a multi-loop linkage with joint clearances," *Mech. Mach. Theory* **43**, 1141–1157 (2008).
26. R. E. Garrett and A. S. Hall, "Effect of tolerance and clearance in linkage design," *Trans. ASME, J. Eng. Ind.* **91**, 198–202 (1969).
27. O. M. A. Sharfi and M. R. Smith, "A simple method for the allocation of appropriate tolerances and clearances in linkage mechanisms," *Mech. Mach. Theory* **18**(2), 123–129 (1983).
28. C. Gosselin, "Determination of the workspace of 6-DOF parallel manipulators," *J. Mech. Des.* **112**, 331–336 (1990).
29. S. Briot and I. A. Bonev, "Accuracy analysis of 3-DOF planar parallel robots," *Mech. Mach. Theory* **43**(4), 445–458 (2008).
30. A. Yu, I. A. Bonev and P. Zsombor-Murray, "Geometric approach to the accuracy analysis of a class of 3-DOF planar parallel robots," *Mech. Mach. Theory* **43**(3), 364–375 (2008).